Received: 22 January 2021 | Accepted: 26 April 2021

DOI: 10.1111/gbi.12449

ORIGINAL ARTICLE

gebiology WILEY

Isotopic analyses of Ordovician–Silurian siliceous skeletons indicate silica-depleted Paleozoic oceans

Elizabeth J. Trower[1] | Justin V. Strauss[2] | Erik A. Sperling[3] | Woodward W. Fischer[4]

[1]Department of Geological Sciences, University of Colorado Boulder, Boulder, CO, USA

[2]Department of Earth Sciences, Dartmouth College, Dartmouth, NH, USA

[3]Department of Geological Sciences, Stanford University, Stanford, CA, USA

[4]Division of Geological and Planetary Sciences, California Institute of Technology, Pasadena, CA, USA

Correspondence
Elizabeth J. Trower, Department of Geological Sciences, University of Colorado Boulder, Boulder, CO, USA.
Email: Lizzy.trower@colorado.edu

Funding information
National Science Foundation, Grant/Award Number: 1624131 and 1922966; Simons Foundation

Abstract

The Phanerozoic Eon marked a major transition from marine silica deposition exclusively via abiotic pathways to a system dominated by biogenic silica sedimentation. For decades, prevailing ideas predicted this abiotic-to-biogenic transition were marked by a significant decrease in the concentration of dissolved silica in seawater; however, due to the lower perceived abundance and uptake affinity of sponges and radiolarians relative to diatoms, marine dissolved silica is thought to have remained elevated above modern values until the Cenozoic radiation of diatoms. Studies of modern marine silica biomineralizers demonstrated that the Si isotope ratios (δ^{30}Si) of sponge spicules and planktonic silica biominerals produced by diatoms or radiolarians can be applied as quantitative proxies for past seawater dissolved silica concentrations due to differences in Si isotope fractionations among these organisms. We undertook 446 ion microprobe analyses of δ^{30}Si and δ^{18}O of sponge spicules and radiolarians from Ordovician–Silurian chert deposits of the Mount Hare Formation in Yukon, Canada. These isotopic data showed that sponges living in marine slope and basinal environments displayed small Si isotope fractionations relative to coeval radiolarians. By constructing a mathematical model of the major fluxes and reservoirs in the marine silica cycle and the physiology of silica biomineralization, we found that the concentration of dissolved silica in seawater was less than ~150 μM during early Paleozoic time—a value that is significantly lower than previous estimates. We posit that the topology of the early Paleozoic marine silica cycle resembled that of modern oceans much more closely than previously assumed.

KEYWORDS

Paleozoic, silica cycle, siliceous sponges, silicon isotopes

1 | INTRODUCTION

The evolution and expansion of silica biomineralization at the beginning of the Paleozoic Era initiated a transformation of the silica cycle from a system governed by strictly abiotic reactions to the biologically dominated cycle that characterizes modern oceans (Tréguer & De La Rocha, 2013). The topology of the silica cycle was fundamentally altered by this biological innovation, including the rates of precipitation, loci of deposition (which would eventually come to reflect the evolution and ecology of silicifying organisms), and the relationship between deposition of organic carbon and silica (Figure S1) (Harrison, 2000; Tréguer, 2002). This transition in the silica cycle is also thought to have affected the concentration of dissolved silica ([DSi]) in seawater. When the silica cycle was

governed solely by abiotic reactions, [DSi] was more tightly controlled by the solubilities of the mineral phases involved, including amorphous silica and various authigenic clays (Siever, 1991,1992). In contrast, the activity of silica biomineralizers has significantly reduced [DSi] below these mineral saturation thresholds, as evident from [DSi] in modern seawater (Gouretski & Koltermann, 2006; Tréguer et al., 1995). Current hypotheses favor a modest decrease in [DSi] to ~500–1000 μM initiated by early silica biomineralizers (i.e., sponges and radiolarians), with a second decrease to modern levels (average [DSi] <10 μM in the surface ocean and ~70 μM in the deep ocean (Tréguer et al., 1995)) occurring much later in the Cenozoic as a consequence of the radiation of diatoms (Figure 1a) (Conley et al., 2017; Harper & Knoll, 1975; Maliva et al., 1989; Racki & Cordey, 2000; Siever, 1991). Others have argued for persistence of Precambrian-like [DSi] values of ~2000 μM until Cretaceous time (Grenne & Slack, 2003). Several recent studies have also speculated that some decreases in seawater [DSi] occurred during Proterozoic time, prior to the evolution of metazoan silica biomineralization, and were driven instead by microbial processes (Conley et al., 2017; Ding et al., 2017). These predictions have not been directly tested due to the lack of a geochemical proxy for [DSi] in ancient seawater.

Previous studies have demonstrated that, in siliceous sponge spicules, the Si isotope fractionation factor (ε^{30}Si)—a metric characterizing the difference in Si isotope ratios (δ^{30}Si) between precipitated silica and seawater DSi—depends strongly on [DSi] in ambient seawater (Figure 1b) (Cassarino et al., 2018; Hendry et al., 2010,2019; Hendry & Robinson, 2012; Wille et al., 2010). This isotopic behavior occurs in members of the Demospongiae and Hexactinellida and contrasts with that observed in diatoms (Cardinal et al., 2005; de la Rocha et al., 1997; Sutton et al., 2013) and inferred in radiolarians (Abelmann et al., 2015), in which ε^{30}Si does not depend on [DSi]. In diatoms, ε^{30}Si is primarily controlled by Si isotope fractionation during cellular uptake via silica transporter proteins; the majority of the DSi that is transported into diatom cells is consumed via polymerization, and there is little DSi efflux (Milligan et al., 2004; Nelson et al., 1976; de la Rocha et al., 1997; Sutton et al., 2013). Although Si isotope fractionation in radiolarians has not been constrained by culturing experiments, δ^{30}Si values of modern and Cenozoic radiolarian tests indicated that ε^{30}Si is similar to that observed in diatoms in both magnitude and independence from [DSi] (Abelmann et al., 2015; Fontorbe et al., 2016,2017,2020). In contrast, Si isotope fractionation in sponges occurs during uptake into, polymerization within, and efflux out of sclerocyte cells (Cassarino et al., 2018; Hendry et al., 2019; Wille et al., 2010). At low [DSi], more of the DSi transported into the sclerocyte is consumed via polymerization, resulting in a small magnitude ε^{30}Si, while at higher [DSi], a smaller proportion of the DSi transported into the sclerocyte is consumed, resulting in a larger magnitude ε^{30}Si (Figure 1b). The ε^{30}Si systematics in modern marine silica biomineralizers appear intrinsic to each clade's distinct body plan and biomineralization pathway such that we can reasonably expect that ancestral silica biomineralizers expressed similar ε^{30}Si-[DSi] relationships.

These ε^{30}Si-[DSi] relationships have been applied to yield a proxy approach to evaluate the [DSi] of ancient seawater from δ^{30}Si measurements of sponge spicules paired with coeval diatoms or radiolarians sampled from Cenozoic strata (Egan et al., 2013; Fontorbe et al., 2016,2017,2020; Hendry et al., 2014). At the elevated [DSi] values hypothesized by Siever (1991) and Conley et al. (2017) for the Paleozoic Era, sponge spiculogenesis is predicted to express a large fractionation factor of $\varepsilon^{30}Si_{sponge}$ ~ −4 to −5‰ (Figure 1b). Interestingly, the limited existing δ^{30}Si data from Cambrian spicular cherts have not revealed any strongly ^{30}Si-depleted isotope ratios

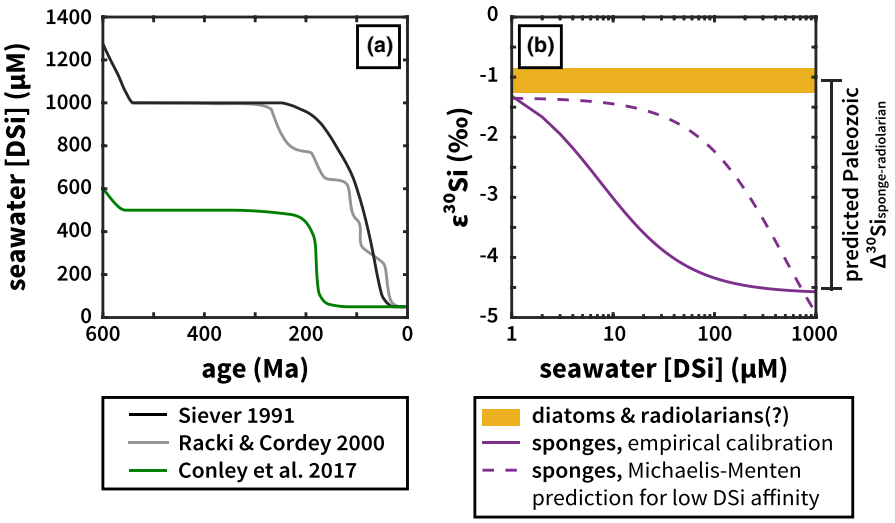

FIGURE 1 (a) Proposed histories of [DSi] over Phanerozoic time (Conley et al., 2017; Racki & Cordey, 2000; Siever, 1991) and (b) relationships of ε^{30}Si versus. [DSi] in sponges. Panel (b) illustrates the most recent empirical calibration of ε^{30}Si based on modern sponges (solid purple line) (Hendry et al., 2019); the diatom ε^{30}Si (Cardinal et al., 2005; de la Rocha et al., 1997; Sutton et al., 2013), assumed to be similar for radiolarians based on modern (Abelmann et al., 2015) and Cenozoic data (Fontorbe et al., 2016,2017,2020) (yellow bar); and an extrapolation of a Michaelis–Menten ε^{30}Si prediction (Cassarino et al., 2018) based on low DSi affinity (dashed purple line)

(Tatzel et al., 2017,2020). To evaluate Paleozoic seawater [DSi], we conducted a suite of ion microprobe $\delta^{30}Si$ and $\delta^{18}O$ analyses of sponge spicules and radiolarians collected from the Ordovician–Silurian Mount Hare Formation of the Road River Group in Yukon, Canada. These isotopic data were supported further by elemental mapping via electron microprobe to evaluate preservation of the geochemical signals. Finally, we constructed a mathematical model that integrates how sponges fractionate silicon isotopes during biomineralization with key fluxes in the marine silica cycle to quantify steady-state [DSi] and $\delta^{30}Si_{DSi}$ under different silica cycle modes. Together, these results revealed estimates of early Paleozoic seawater [DSi] values that are relatively similar to those in modern oceans, demonstrating that Paleozoic silica-biomineralizing organisms controlled the marine silica cycle just as strongly as diatoms do today.

2 | MATERIALS AND METHODS

2.1 | $\delta^{30}Si$ and $\delta^{18}O$ isotopic analyses

Four polished 1-inch round thin sections were mounted in epoxy with grains of the Caltech Rose Quartz reference material ($\delta^{30}Si = 0.02‰$, $\delta^{18}O = 8.45‰$; (Georg et al., 2007)) by High Mesa Petrographics (White Rock, NM). Thin sections were imaged using transmitted and reflected light and coated in Au (30 nm thick) prior to isotopic analysis. $\delta^{30}Si$ and $\delta^{18}O$ measurements were conducted using a Cameca IMS 7f-GEO secondary ion mass spectrometer (SIMS) at the Caltech Microanalysis Center during a single session in November 2017, following methods detailed in Stefurak et al. (2015). $\delta^{30}Si$ and $\delta^{18}O$ were measured separately, using O^- (3–4 nA with 9 kV acceleration) and Cs^+ (2–4 nA with 9 kV acceleration) primary ion beams, respectively, since the achievable precision for $\delta^{30}Si$ with the IMS 7f-GEO was observed to be better using this method than using dynamic peak hopping to measure both $\delta^{30}Si$ and $\delta^{18}O$ with the Cs^+ beam (Stefurak et al., 2015). Mass resolving power of *ca.* 2,400 was achieved for $\delta^{30}Si$ analyses (sufficient for excluding contributions from the $^{29}Si^1H$ hydride peak in ^{30}Si measurements) and *ca.* 1,200 for $\delta^{18}O$ analyses. Although ^{16}O implantation by the O^- beam during $\delta^{30}Si$ analyses was not previously found to affect subsequent $\delta^{18}O$ analyses, we erred on the side of caution by analyzing $\delta^{18}O$ prior to $\delta^{30}Si$ on each sample. The focused ion beam was rastered across an area for each measurement, producing effective analyzed areas of ~30–40 μm in width. Each analysis included pre-sputtering (60 s for $\delta^{30}Si$, 90 s for $\delta^{18}O$), field centering, and analyses (20 cycles, $\delta^{30}Si$ count times: 0.96 s for ^{28}Si and 8.00 s for ^{30}Si, $\delta^{18}O$ count times: 0.96 s for ^{16}O and 4.96 s for ^{18}O). Sets of 7–14 sample spots were bracketed by 4–5 repeat analyses of the reference material (Caltech Rose Quartz) (Figure S2). Typical measurement precision was ±0.3‰ (1σ) for $\delta^{18}O$ measurements and ±0.2 to 0.3‰ (1σ) for $\delta^{30}Si$ measurements. Isotope ratios are reported as permil deviations from VSMOW (Vienna Standard Mean Ocean Water) for oxygen and the NBS-28 quartz standard (defined as 0‰) for silicon using delta notation.

2.2 | Microscopy

Thin sections were examined in transmitted and reflected light via petrographic microscope prior to and after SIMS analysis. Raman microspectroscopic analyses were performed using a Horiba LabRAM HR Evolution Spectrometer with a 532 nm excitation laser at the CU Boulder Raman Microspectroscopy Lab to determine SiO_2 mineralogy (e.g., opal-A, opal-CT, quartz) and screen fossil specimens for presence of structural water in the form of silanol bonds (apparent as a peak at 503 cm^{-1} (Schmidt et al., 2012)). Elemental maps characterizing the distributions of Si, Al, Mg, K, and Fe were collected using a JEOL 8230 Superprobe at the CU Boulder Electron Microprobe (EMP) laboratory. The thin Au coatings were removed via gentle polishing prior to re-coating with C before EMP analysis. Qualitative intensity maps without background corrections via wavelength dispersive X-ray spectrometry (WDS) were collected at 15 kV accelerating voltage, 11 mm working distance, 30 nA beam current, and 100 ms dwell time.

2.3 | Geochemical modeling

We constructed a simple mathematical model of the marine silica cycle to constrain the set of conditions necessary to match observed $\Delta^{30}Si_{sponge\text{-}radiolarian}$ values by modifying a simple two-box model of the marine silica cycle (capturing surface and deep seawater reservoirs) based on previous work (Frings et al., 2016; De La Rocha & Bickle, 2005). With this framework, we compared different scenarios of BSi production to determine which one best fit our observed $\Delta^{30}Si_{sponge\text{-}radiolarian}$ values: (1) a modern scenario with diatoms in the surface ocean and sponges in the deep ocean ("diatom +sponge"); (2) a non-planktonic scenario with benthic BSi production by sponges as the only silica sink ("sponge-only"); and (3) a Paleozoic scenario with radiolarians in the surface ocean and sponges in the deep ocean ("sponge + radiolarian") (Figure S3a). Within the sponge + radiolarian scenario, we compared model predictions using different DSi utilization kinetics (conservative DSi affinity from measurements of modern sponges vs. DSi affinity >20-fold lower than observed in any modern sponges) and different parameterizations of the $\varepsilon^{30}Si$-[DSi] relationship (the modern empirical calibration (Hendry et al., 2019) vs. a Michaelis–Menten model of $\varepsilon^{30}Si$ for the hypothetical low DSi affinity sponge scenario (Cassarino et al., 2018); Figure 1b).

Model input parameters are provided in Table S1. Models were initialized with surface and deep ocean [DSi] =500 μM and iterated with 0.1 yr timesteps until they reached steady state. The duration required to reach steady state depended on initial conditions (models with lower DSi uptake affinity required more time to reach steady state). We used these models to compare predictions of steady-state [DSi], $\delta^{30}Si_{seawater}$, and $\delta^{30}Si_{BSi}$ of different BSi sinks for a suite of input fluxes and $\delta^{30}Si_{input}$ with observed Paleozoic $\delta^{30}Si_{BSi}$ and $\Delta^{30}Si_{sponge\text{-}radiolarian}$ values. The diatom + sponge model was parameterized following Frings et al. (2016), with the addition of BSi production by sponges in the

deep oceans using a conservative estimate of Michaelis–Menten kinetics from sponge physiological data (i.e., modern sponges with a low affinity for DSi) (López-Acosta et al., 2018; Maldonado et al., 2011) and assuming negligible spicule dissolution prior to sedimentation (Chu et al., 2011; Erez et al., 1982; Kamatani, 1971; Maldonado et al., 2005). We applied the most recent modern calibration of the ε^{30}Si-[DSi] relationship to calculate sponge ε^{30}Si as a function of [DSi] (Hendry et al., 2019). In the sponge-only model, we implemented seafloor BSi production by sponges as the sole silica sink, using the same parameterization in the diatom + sponge model but with a greater percentage of the seafloor colonized by sponges (Table S1). In the sponge + radiolarian model, we added BSi production by radiolarians in the surface ocean with dissolution during sinking—a topology analogous to the modern diatom + sponge model. Although the DSi uptake kinetics of radiolarians are unknown, we assumed Michaelis–Menten kinetics identical to sponges (i.e., radiolarians, like sponges, are less efficient at DSi utilization than diatoms). This assumption was supported by the observation that diatoms outcompete radiolarians as the primary planktonic BSi producers in modern oceans (Tréguer & De La Rocha, 2013); assigning radiolarians with similar DSi uptake kinetics to diatoms reproduces the topology and results of the diatom + sponge model. We applied a lower dissolution rate of radiolarians relative to diatoms in the deep oceans based on modern observations (Berger, 1968; Erez et al., 1982), and we assumed radiolarians have a similar ε^{30}Si-[DSi] relationship to diatoms (i.e., ε^{30}Si = −1.1‰, independent of [DSi]), which is supported by modern and Cenozoic δ^{30}Si data (Abelmann et al., 2015; Fontorbe et al., 2016 2017 2020). Finally, we varied Michaelis–Menten parameters (V_{max} and K_m) to decrease DSi affinity (V_{max}/K_m) in the sponge + radiolarian model to quantify the conditions required to sustain [DSi] at the levels predicted by Siever (1991) and Conley et al. (2017) for Paleozoic seawater. We also compared versions of this low DSi affinity model with the empirical $\varepsilon^{30}Si_{sponge}$ calibration (Hendry et al., 2019) and a Michaelis–Menten $\varepsilon^{30}Si_{sponge}$-[DSi] relationship (Cassarino et al., 2018).

3 | RESULTS

3.1 | Geological context and microscopy

The Mount Hare Formation is a >700 m thick sedimentary succession of interbedded shale, limestone, and chert, within the Road River Group, a widespread basinal lithostratigraphic unit in northwestern Canada. Specifically, we studied the section exposed on the upper canyon of the Peel River in the Richardson Mountains, Yukon, Canada (Figure S4). These strata reflect lower slope to basin-floor deposits of the Richardson trough—an intraplatformal basin on the edge of the Great American Carbonate Bank (Lenz, 1972; Morrow, 1999; Strauss et al., 2020). Rocks from this region are mature to overmature with respect to oil generation, based on conodont alteration indices (CAI) ranging from 2–6 in our section and regional vitrinite reflectance values ranging from 2.21% to 3.86%Ro_R (Fraser et al., 2012; Link & Bustin, 1989; Strauss et al., 2020).

Samples were selected from a section of the Mount Hare Formation spanning the Middle Ordovician through Lower Silurian: one Darriwilian sample, one upper Katian sample, and two Llandovery samples (stratigraphic heights 48.7, 92.4, 167.9, and 187.4 m in Strauss et al. (2020) section J1518, respectively) (Figure S4). The samples were composed of siliceous fossils suspended in a matrix of dark, organic-rich chert. The spicules in our samples were mostly simple monaxons, including styles, strongyles, and tylotes, with rare triaxons (hexactine and triradiate spicules). The latter are consistent with origins from taxa within the class Hexactinellida, but the monaxon spicules likely originated from members of the Demospongiae. Radiolarian skeletons were circular in cross-section and ~100 μm in diameter; in some specimens, the outer test wall was optically distinguishable from the interior cavity, which was filled with silica cement during diagenesis. Light microscopy and Raman microspectroscopy demonstrated that the fossils have all been transformed to chalcedony (fibrous quartz) or microquartz, with no detectable structural water (silanol bonds) (Figure 2a).

Early diagenetic alteration of biogenic silica (BSi) to authigenic clay minerals via reverse weathering reactions is an important process that commonly affects diatoms; evidence of this alteration can be observed as rims with elevated abundances of Al, K, Mg, and Fe surrounding the diatom frustule (Koning et al., 2007; Loucaides et al., 2010; Michalopoulos & Aller, 2004; Michalopoulos et al., 2000). There is some evidence that authigenic clay minerals produced by these secondary reactions could lower δ^{30}Si values from the primary BSi composition (Tatzel et al., 2015). To test for this, electron microprobe mapping on the samples examined herein revealed that this type of alteration did not occur in the spicules and radiolarians we measured for isotopic data (Figure 2b, Figure S5). Although trace clay minerals (evidenced by higher abundances of Al and K) occur in the surrounding chert matrix, these enrichments are notably absent within the examined spicules and radiolarians. Moreover, we observed no authigenic clay rims analogous to those observed in the alteration of modern diatoms. Maps of Ca and Mg revealed rare, disseminated euhedral carbonate rhombs within the chert matrix, and maps of Fe displayed the presence of rare pyrite within the chert matrix (Figure 2b, Figure S5); neither carbonate nor pyrite minerals were spatially associated with the spicules or radiolarians.

3.2 | δ^{30}Si and δ^{18}O

During diagenesis, primary biogenic silica (composed of opal-A) is typically transformed first to opal-CT, then to microcrystalline quartz (i.e., chert). The rate, timing, and style of these reactions are variable and depend on sediment mineralogy (e.g., clay-rich vs. carbonate-rich), geothermal gradient and burial history, and fossil type (e.g., sponge spicules are more resistant to dissolution than diatoms) (Williams & Crerar, 1985; Williams et al., 1985; Yanchilina et al., 2020). These diagenetic stabilization reactions

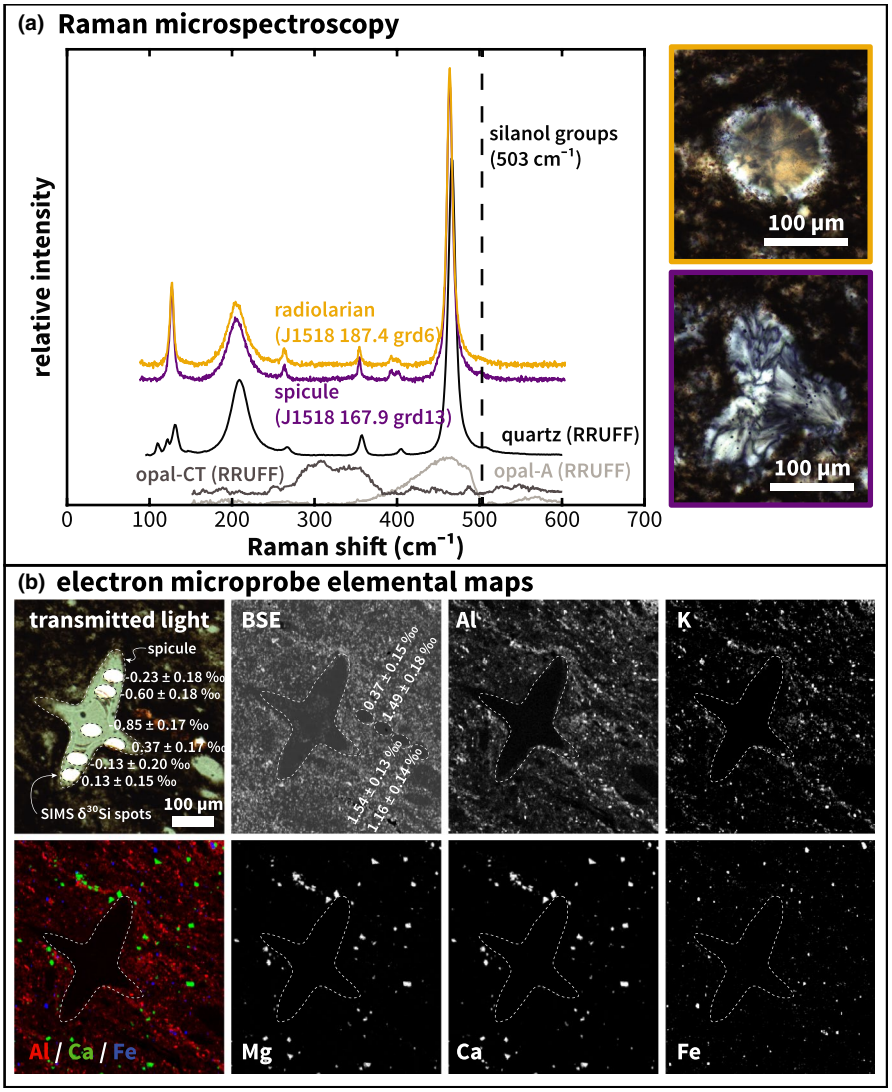

FIGURE 2 Microscopy and chemical imaging of radiolarians and sponge spicules from Mount Hare Formation samples. (a) Cross-polarized light microscopy and Raman microspectroscopy data illustrating composition of spicules and radiolarian tests. Right: cross-polarized light microscopy images of radiolarian (top, yellow outline) and spicule (bottom, purple outline), demonstrated that fossils have transformed to chalcedony (fibrous quartz) during diagenesis, based on characteristic extinction patterns. Left: Raman spectra of radiolarian test (yellow line) and spicule (purple line), corresponding to the two fossils shown in the right panels, compared with standard materials: quartz (black line), opal-CT (medium gray line), and opal-A (light gray line) from the RRUFF database, demonstrating that fossils are now composed of quartz. We did not observe a characteristic peak at 503 cm^{-1} (Schmidt et al., 2012), which indicates the presence of structural water in the form of silanol moieties, in any of the samples analyzed. (b) Electron microprobe elemental data of sponge spicule from sample J1518-48.7. δ^{30}Si values with 1σ standard deviations are overlain on transmitted light image (spots within spicule) and back-scattered electron (BSE) image (spots within matrix); spicule δ^{30}Si values (mean δ^{30}Si −0.22‰, $n = 6$) contrast strongly with δ^{30}Si values of the adjacent chert matrix (mean δ^{30}Si 1.14‰, $n = 4$). The remaining panels illustrate WDS data: maps of elements Al, K, Mg, Ca, and Fe, and an RGB map plotting Al (red), Ca (green), and Fe (blue)

occur at relatively shallow burial depths and low temperatures. In clay-rich sediments, both opal-A→opal-CT and opal-CT→quartz transformations are dissolution–reprecipitation reactions (Kastner et al., 1977; Murata et al., 1977; Yanchilina et al., 2020), in which there is potential for exchange and re-equilibration of O isotopes with local pore fluids. However, the opal-A→opal-CT transition can occur very rapidly in carbonate-rich environments (Kastner et al., 1977): recent evidence showed preservation of δ^{18}O values in opal-CT that were closer to primary opal-A δ^{18}O than to expected equilibrium δ^{18}O values (Yanchilina et al., 2021). Furthermore, experimental work has indicated that the opal-CT→quartz transition in carbonate-rich sediments may occur as a solid-state reaction (Ernst & Calvert, 1969), in which O isotope exchange with porewaters would occur to a much lower degree. Our samples were collected from an originally carbonate-rich section (Figure S4), suggesting that O isotope exchange may have occurred to a limited extent. However, given the complex relationship between δ^{18}O transformations and paragenetic sequence, δ^{18}O values here were primarily applied as

a screening tool rather than as a record of seawater $\delta^{18}O$ values. Previous studies have demonstrated preservation of primary $\delta^{30}Si$ variability in Archean and Proterozoic chert-rich metasediments even when $\delta^{18}O$ values have been altered during diagenesis (Heck et al., 2011; Marin-Carbonne et al., 2012; Stefurak et al., 2015) because $\delta^{30}Si$ values are far better sediment-buffered and therefore more resistant to alteration than $\delta^{18}O$ values, which tend to be fluid-buffered. In other words, diagenetic transformations tend to act as closed systems with respect to $\delta^{30}Si$ because the mass balance of Si is dominated by Si in sediments » Si in pore fluids (i.e., "sediment-buffered"). This contrasts starkly with the behavior of $\delta^{18}O$, which tends to be comparatively fluid-buffered and thus can be more readily altered, with the exact mass balance between sediment and pore fluids determined by water/rock ratios during burial.

The mean $\delta^{18}O$ value of sponge spicules was 26.6‰ (standard deviation 2.6‰, range 23.6 to 31.7‰) (Figure 3, Table S2), similar to $\delta^{18}O$ values previously reported from early Paleozoic chert successions (Chen et al., 2020; Degens & Epstein, 1962; Jones & Knauth, 1979; Karhu & Epstein, 1986; Knauth & Epstein, 1976). Previous studies of $\delta^{18}O$ in siliceous spicules have revealed that substantial vital effects are imparted during the biosynthesis of these materials. These data illustrated considerable variability (up to 5‰)

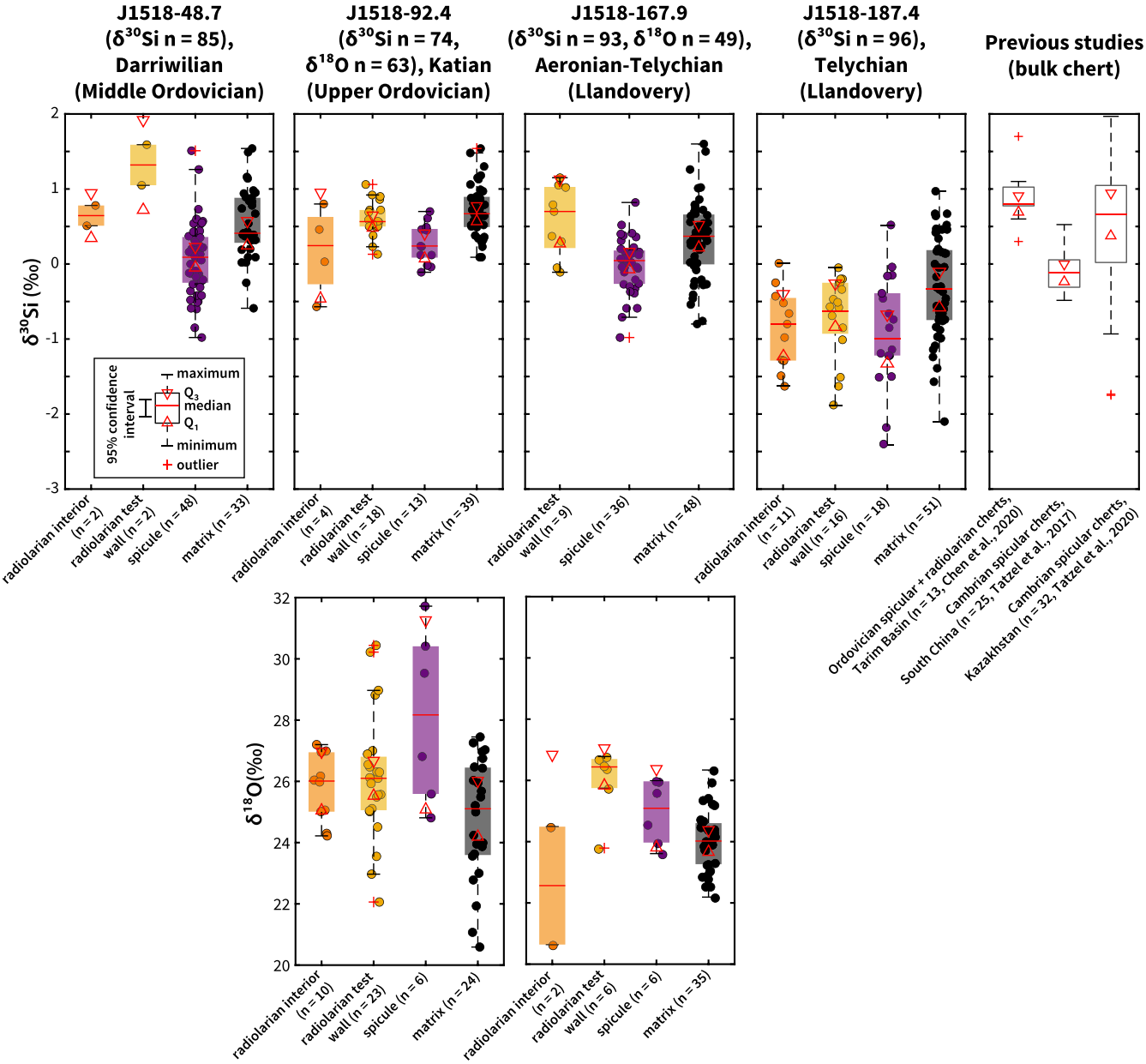

FIGURE 3 Box plots of distributions of SIMS $\delta^{30}Si$ and $\delta^{18}O$ values of radiolarians, sponge spicules, and chert matrix from the Mount Hare Formation samples. Bulk $\delta^{30}Si$ data from Cambrian and Ordovician spicular cherts (Chen et al., 2020; Tatzel et al., 2017,2020) are plotted for comparison. For [DSi] ≥500 μM and observed $\delta^{30}Si_{radiolarian}$ ≤1.5‰, $\delta^{30}Si_{sponge}$ should be ≤−3‰ (Figure 1b). Data points identified as "outliers" in the box plots are outside 1.5 times the interquartile range; however, these data points are all included in the statistics and statistical analyses in Table S2 and Figures S10–S11

within individual sponge species grown under the same conditions, indicating that spicules do not form in oxygen isotope equilibrium with ambient water (Matheney & Knauth, 1989; Matteuzo et al., 2013; Snelling et al., 2014). We interpreted the observed $\delta^{18}O$ range in spicules as both primary $\delta^{18}O$ variability combined with a lowering of $\delta^{18}O$ values during diagenetic recrystallization from amorphous silica to microquartz (Jones & Knauth, 1979). The $\delta^{18}O$ values of radiolarian test walls and sponge spicules tended to be higher than those of the chert matrix (Figure 3)—a pattern consistent with the view of better preservation of primary isotope signals in biogenic silica than in the chert matrix. The preservation of $\delta^{18}O$ heterogeneity in the Mount Hare samples (Figure 3) therefore also supported the interpretation that primary $\delta^{30}Si$ values are well-preserved.

The $\delta^{30}Si$ values of sponge spicules from the Mount Hare Formation ranged from −2.4 to 1.5‰, with $\delta^{30}Si$ values in sample J1518-187.4 (median $\delta^{30}Si$ = −1.0‰) recording significantly lower values than the other three samples (median $\delta^{30}Si$ = 0.1, 0.24, and 0.1‰) at the 95% confidence level (Figure 3, Figures S6–S11, Table S2, Dataset S1). Analytical spots located on the test walls of radiolarian skeletons displayed higher $\delta^{30}Si$ values than spots on the interiors (Figure 3, see also grd6/grd6b in Figure S7); this pattern most likely reflects porewater and/or early diagenetic $\delta^{30}Si$ values because the interiors of radiolarian skeletons are hollow and were filled with silica cement prior to compaction. The median $\delta^{30}Si$ values of radiolarian test walls and interiors were not significantly different at the 95% confidence level in any sample (Figure 3), but in three of the four samples, the median $\delta^{30}Si$ values of radiolarian test

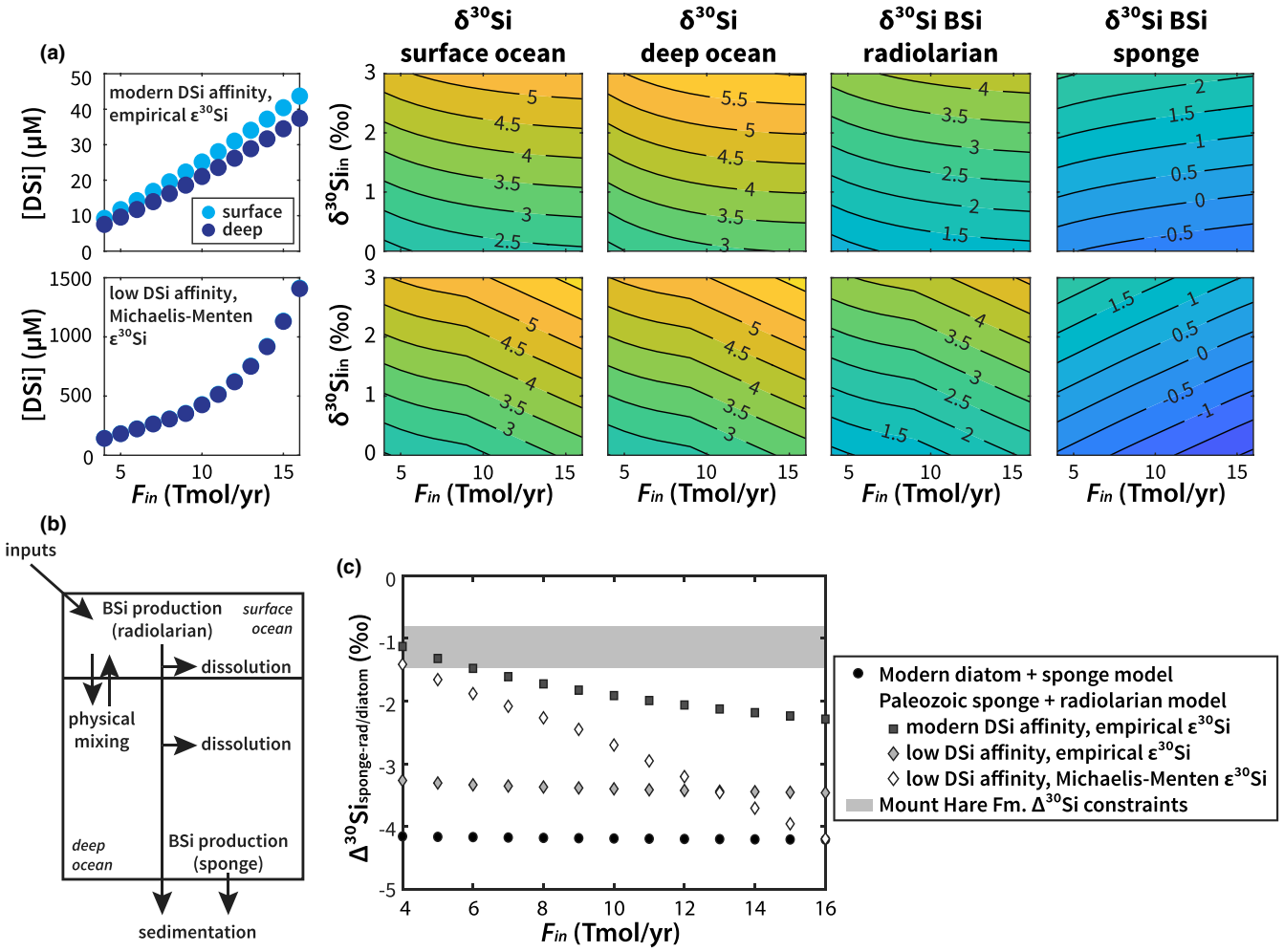

FIGURE 4 Results of geochemical modeling of early Paleozoic [DSi] and $\delta^{30}Si$. (a) Model predictions: scatter plots of [DSi] for surface and deep oceans and contour plots $\delta^{30}Si$ values of surface ocean, deep ocean, planktonic silica biomineralizers (radiolarians), and sponges for the two most realistic versions of the model, from top to bottom: (1) sponge + radiolarian assuming modern DSi affinity and modern empirical $\varepsilon^{30}Si$-[DSi] calibration; and (2) sponge + radiolarian assuming 20x lower DSi affinity than modern sponges and Michaelis–Menten $\varepsilon^{30}Si$-[DSi] prediction. All plots share the same color scale. Predictions of additional versions of the model discussed in the text are illustrated in Figure S3. (b) Schematic illustration of mathematical model for the Paleozoic marine silica cycle; additional arrangements of the model discussed in the text are illustrated in Figure S3. (c) Comparison of model predictions of steady-state $\Delta^{30}Si_{sponge\text{-}diatom/radiolarian}$ (scatter plot) with $\Delta^{30}Si_{sponge\text{-}radiolarian}$ constraints from SIMS data from Mount Hare Formation (Fm.) samples (gray box)

walls and sponge spicules were significantly different at the 95% confidence level (Figure 3). The $\delta^{30}Si$ population means of radiolarian test walls and sponge spicules pooled across these three samples (excluding J1518-187.4) were also significantly different at the 95% confidence level (Figure S11). $\Delta^{30}Si_{sponge\text{-}radiolarian}$ values—calculated as the difference between median $\delta^{30}Si$ values of spicules and radiolarian test walls—displayed a small range from −0.33 to −1.23‰ (Table S2). If we accepted that the maximum $\delta^{30}Si$ values of radiolarian test walls may more accurately reflect primary values due to the lowering of $\delta^{30}Si$ values due to mixing during diagenesis, which was evidenced by the offset between radiolarian test walls and interiors, calculated $\Delta^{30}Si_{sponge\text{-}radiolarian}$ values range from −0.82 to −1.50‰ (Table S2). The chert matrices displayed similar $\delta^{30}Si$ values to spicules and radiolarian test walls (Figure 3, Figure S10–S11), consistent with the matrix forming via diagenetic remobilization of primary BSi. The greater extent of overlap in $\delta^{30}Si$ values among the various phases and noticeably lower $\delta^{30}Si$ values in sample J1518-187.4 across all microfabric types implied that the fossils in this sample may have experienced a greater extent of diagenetic alteration than the other three samples (Figure 3, Figure S10–S11). In the other three samples, we interpreted that primary $\delta^{30}Si$ values of spicules and radiolarian tests were well-preserved, based on heterogeneity of $\delta^{18}O$ values (which are more fluid-buffered during diagenesis), systematic $\delta^{30}Si$ offsets between materials that were consistent with expected differences in $\varepsilon^{30}Si$ and paragenesis, and current understanding of the divergent behavior of $\delta^{30}Si$ and $\delta^{18}O$ during diagenesis.

3.3 | Quantifying early paleozoic [DSi] and $\delta^{30}Si$

The $\Delta^{30}Si_{sponge\text{-}radiolarian}$ values we observed did not match the magnitude predicted based on prevailing ideas about high Paleozoic seawater [DSi] (Figure 1b), indicating that the standing stock of silica in the oceans was lower than expected. But by how much? Predictions from the diatom + sponge model matched the characteristics of the modern silica cycle in terms of [DSi] in the surface and deep ocean and $\delta^{30}Si$ values of DSi and BSi for modern input fluxes (F_{in} and $\delta^{30}Si_{in}$; Figure S3). The sponge + radiolarian model scenario, assuming modern sponge DSi affinities and $\varepsilon^{30}Si$-[DSi] calibrations, predicted surface and deep ocean [DSi] <50 μM (Figure 4a, Figure S3)—values far lower than hypotheses of 500–1,000 μM (Conley et al., 2017; Siever, 1991). The low DSi affinity sponge + radiolarian model scenario generated [DSi] predictions closer to those of Siever (1991) and Conley et al., (2017), although only for F_{in} >10 Tmol/yr (Figure 4a, Figure S3). Models with even more extreme Si utilization kinetics failed to reach steady state because BSi production could not keep up with the input flux, F_{in}, and the models do not include abiotic solubility-controlled precipitation of amorphous silica (Figure S12).

These model scenarios generated different predictions of $\Delta^{30}Si_{sponge\text{-}diatom/radiolarian}$, the offset in $\delta^{30}Si$ values between sponges and planktonic BSi (diatoms or radiolarians, depending on the model) (Figure 4c). All sponge + radiolarian models predicted that more of the net BSi output was partitioned into spicules than radiolarians across most of the parameter space we explored (Figure S12), except for combinations of low DSi affinity and very high F_{in}. This was a consequence of the differences in dissolution (radiolarians were allowed to dissolve as they sink; sponges were assumed to be buried with negligible dissolution). As the contrast in $\Delta^{30}Si$ values between the sponge + radiolarian models and the diatom + sponge model demonstrated, this topology was required to attain both a smaller magnitude value of $\Delta^{30}Si$ and $\delta^{30}Si_{sponge}$ ~0‰ (Figure 4c, Figure S3,S12). Models with combinations of low DSi affinity and very high F_{in} predicted steady-state [DSi] ≥1,000 μM, but also large magnitudes of $\Delta^{30}Si_{sponge\text{-}radiolarian}$ and $\delta^{30}Si_{sponge}$ >0‰—both of which are inconsistent with our observations from Mount Hare Formation samples.

4 | DISCUSSION

The Ordovician–Silurian $\Delta^{30}Si_{sponge\text{-}radiolarian}$ values determined here differ markedly from $\Delta^{30}Si_{sponge\text{-}diatom}$ values observed in modern oceans (Figure S3) or predicted by results from the Modern diatom + sponge silica cycle model (Figure 4c). The preservation of $\delta^{30}Si$ and $\delta^{18}O$ heterogeneity in the Mount Hare samples precluded substantial $\delta^{30}Si$ resetting during diagenesis that could have erased a larger original $\Delta^{30}Si_{sponge\text{-}radiolarian}$ signal. In addition, electron microprobe elemental maps of the Mount Hare samples revealed no evidence of alteration to authigenic clay minerals. Carbonate and organic carbon isotope chemostratigraphic data from the Road River Group in the Richardson trough displayed multiple globally recognized isotopic excursions (Strauss et al., 2020), indicating that the basin was in communication with global oceans and that our $\delta^{30}Si$ data are unlikely to reflect only local basinal effects. Chen et al. (2020) reported bulk $\delta^{30}Si$ values ranging from 0.3 to 1.7‰ in spicule- and radiolarian-bearing Darriwilian (Middle Ordovician) chert from the Tarim Basin in China. These data were remarkably consistent with our SIMS $\delta^{30}Si$ data (Figure 3) and indicated that this pattern is not unique to the Richardson trough. We therefore concluded that our $\Delta^{30}Si_{sponge\text{-}radiolarian}$ estimates reflect primary environmental signals.

$\delta^{30}Si$ data from early Cambrian spicular chert in South China and Kazakhstan also display similar signals to the SIMS $\delta^{30}Si_{sponge}$ data presented here (Figure 3). Bulk $\delta^{30}Si$ values in spicular chert of the Liuchapo and Xiaoyanxi formations (South China) range from −0.5 to 0.5‰ (mean −0.1‰) (Tatzel et al., 2017) and bulk $\delta^{30}Si$ values in spicular chert of the Chulaktau Formation (Kazakhstan) ranged from −1.8 to 2.0‰ (mean 0.5‰) (Tatzel et al., 2020). These data were originally interpreted to reflect mixing of a relatively small proportion of sponge spicules (assumed to have $\delta^{30}Si_{sponge}$ = −4 to −5‰) with detrital silicate minerals, authigenic clay, and abiotic silica precipitated from seawater. However, thin sections from these studies reveal abundant spicules and putative radiolarians and mass balance calculations assume $\varepsilon^{30}Si_{abiotic\ silica\text{-}DSi}$ = 0‰ (Tatzel et al., 2017), even though most studies of $\delta^{30}Si$ systematics from Precambrian chert have suggested $\varepsilon^{30}Si_{abiotic\ silica\text{-}DSi} \cong$ −1‰ (Geilert et al., 2014; Li et al., 1994; Roerdink et al., 2015; Stefurak et al., 2015). Our model results indicated that

these data are better interpreted as a reflection of $\delta^{30}Si_{sponge}$ values near 0‰, consistent with steady-state $\delta^{30}Si_{sponge}$ predictions for near-modern $\delta^{30}Si_{inputs}$ from sponge-only, sponge + radiolarian, and low DSi affinity sponge + radiolarian models (Figure 4a, Figure S3). Under this interpretation, these data extend the evidence of low seawater [DSi] further back in time, close to the Precambrian–Cambrian boundary. Furthermore, even in low DSi affinity sponge + radiolarian box models, steady-state $\delta^{30}Si_{sponge} \cong \delta^{30}Si_{inputs}$ and $\delta^{30}Si_{inputs}$ >0‰ due to the formation of secondary clay minerals during silicate weathering (Pogge von Strandmann et al., 2012; Ziegler et al., 2005; Ziegler et al., 2005). Consequently, $\delta^{30}Si_{sponge} = -4$ to −5‰ could only transiently characterize spicules while [DSi] was still constrained by mineral solubilities (>1,000 μM) (Figure S3), but the first appearance of silica-biomineralizing sponges could be marked by a brief negative excursion in the $\delta^{30}Si_{chert}$ record. SIMS-scale analyses enabled us to avoid the potentially confounding effects of mixing $\delta^{30}Si$ signals of different sedimentary components in bulk $\delta^{30}Si$ analyses and suggest that published bulk $\delta^{30}Si$ values of early Paleozoic spicular cherts may be more representative of BSi $\delta^{30}Si$ values than originally assumed.

The $\Delta^{30}Si_{sponge\text{-}radiolarian}$ estimates from our SIMS analyses are consistent with the predictions of the sponge + radiolarian box model, and in particular, either (1) modern-like DSi affinities and modern empirical $\varepsilon^{30}Si$ calibrations; or (2) DSi affinity 20x lower than the lowest modern values and an extrapolated Michaelis–Menten $\varepsilon^{30}Si$ prediction (Figure 4c, Figure S3). Both scenarios require substantially lower steady-state seawater [DSi] than previous predictions (Figure 1a). This indicated that early silica biomineralizers were more effective at drawing down DSi than previously hypothesized and that any reduction in [DSi] caused by the Cenozoic radiation of diatoms was much smaller in magnitude than previously hypothesized.

It has been observed that modern sponge silica uptake kinetics appear poorly adapted to modern seawater [DSi], causing sponges to experience chronic DSi limitation: the experimentally determined concentrations (K_m) at which sponge Si utilization is half its maximum value (V_{max}) are much lower than [DSi] values that characterize sponge habitats (López-Acosta et al., 2016,2018; Maldonado et al., 2011; Reincke & Barthel, 1997). This observation was interpreted to indicate that modern sponge DSi kinetics may have been inherited from Paleozoic sponges (Maldonado et al., 2011). Instead, our results suggest that sponge DSi kinetics may have been set during the early evolution of spicules in the Tonian–Ediacaran Periods (Sperling et al., 2010) when [DSi] was much higher. Regardless of the exact DSi affinities, our results suggested that the early Paleozoic marine silica cycle more closely resembled the modern system than previously assumed in terms of the extent of control by silica biomineralizers, with the notable difference that BSi output was partitioned more into benthic BSi (spicules) than planktonic BSi (radiolarians), in contrast with the modern system in which planktonic BSi (diatoms) dominate BSi output (Tréguer & De La Rocha, 2013).

Our $\Delta^{30}Si_{sponge\text{-}radiolarian}$ SIMS data and model results also have implications for processes behind silica inputs to the ocean—processes that matter for the carbon cycle, climate, and weathering. Model results indicated that the silica inputs to the oceans were lower than today, and the isotopic composition of this input was modestly lower than the modern value (Figure 4a, Figure 4c). Both features are consistent with a lower extent of terrestrial silicate weathering at this time. While rates of silicate weathering reflect a complex, interwoven suite of processes involved in global tectonic processes (uplift and erosion, production and inversion of sedimentary basins, outgassing, and metamorphism), (Berner & Caldeira, 1997; Broecker & Sanyal, 1998; Zeebe & Caldeira, 2008), our findings are consistent with previous ideas about differences in the efficiency of silicate weathering prior to the Devonian expansion of vascular land plants. Lower marine $\delta^{30}Si_{input}$ values suggested a smaller extent of secondary clay formation during silicate weathering, which may have been driven by less intense weathering and/or shallower weathering profiles (Pogge von Strandmann et al., 2012; Ziegler, Chadwick, Brzezinski, et al., 2005; Ziegler, Chadwick, White, et al., 2005). This interpretation is consistent with the low abundance of alluvial mudrock in Ordovician–Silurian relative to Devonian–Carboniferous sedimentary successions (Davies & Gibling, 2010; McMahon & Davies, 2018), reflecting different weathering processes prior to the Devonian expansion of vascular land plants (Algeo et al., 1995; Berner, 1992; Boyce & Lee, 2017; Gibling & Davies, 2012; Ibarra et al., 2019; McMahon & Davies, 2018). Although the relatively short duration of time spanned by our sample set makes it challenging to uniquely identify the cause(s) of low early Paleozoic DSi fluxes, we posit that the following factors could have contributed: (1) reduced solute fluxes due to the timing of deposition predating the expansion of vascular land plants, as observed in barren modern landscapes (Moulton et al., 2000); (2) reduced weathering rates due to the transition into a colder global climate state (Bergmann et al., 2018; Finnegan et al., 2011; Trotter et al., 2008); and (3) reduced weathering rates due to Ordovician–Silurian paleogeography, with the supercontinent Gondwana concentrating continental landmasses at high southern latitudes (Cocks & Torsvik, 2002; Crowley & Baum, 1995). Notably, both lower $\delta^{30}Si_{input}$ values and lower DSi input fluxes implicate the evolutionary history of plants having some influence on the marine silica cycle. Additional analyses of $\Delta^{30}Si_{sponge\text{-}radiolarian}$ values spanning the entirety of the Paleozoic Era could provide a refined tool to track changes in fluxes and $\delta^{30}Si$ values of DSi input and more robustly deconvolve the hypothesized effects of the evolution and expansion of land plants on silicate weathering from tectonic and/or climatic influences.

ACKNOWLEDGMENTS

The authors thank Yunbin Guan (Caltech), Aaron Bell (University of Colorado Boulder), and Eric Ellison (University of Colorado Boulder) for assistance with SIMS, EMP, and Raman microspectroscopy analyses, respectively, and Michael Melchin (St. Francis Xavier University) and Tiffani Fraser (Yukon Geological Survey) for assistance studying the Peel River section. The authors thank Johanna Marin-Carbonne and three anonymous reviewers for their constructive comments. E. J. T acknowledges support from

the Agouron Institute Geobiology Postdoctoral Fellowship. J. V. S. and E. A. S. were supported by National Science Foundation (NSF) grants EAR-1624131 and EAR-1922966, respectively, along with additional support from the Yukon Geological Survey. W. W. F. was supported by the Simons Foundation Collaboration on the Origins of Life, the GPS Discovery Fund, and the Caltech Center for Evolutionary Sciences.

DATA AVAILABILITY STATEMENT

MATLAB code for each silica cycle model scenario is archived at: https://doi.org/10.5281/zenodo.4632430. SIMS analysis maps, SIMS data, and EMP maps are archived at: https://doi.org/10.17605/OSF.IO/4AES6.

ORCID

Elizabeth J. Trower https://orcid.org/0000-0001-9898-5589
Justin V. Strauss https://orcid.org/0000-0003-3298-3227
Erik A. Sperling https://orcid.org/0000-0001-9590-371X
Woodward W. Fischer https://orcid.org/0000-0002-8836-3054

REFERENCES

Abelmann, A., Gersonde, R., Knorr, G., Zhang, X., Chapligin, B., Maier, E., Esper, O., Friedrichsen, H., Lohmann, G., Meyer, H., & Tiedemann, R. (2015). The seasonal sea-ice zone in the glacial Southern Ocean as a carbon sink. *Nature Communications*, *6*, 8136. https://doi.org/10.1038/ncomms9136

Algeo, T. J., Berner, R. A., Maynard, J. B., & Scheckler, S. E. (1995). Late devonian oceanic anoxic events and biotic crises: "rooted" in the evolution of vascular plants. *GSA Today*, *5*(3), 45–66.

Berger, W. H. (1968). Radiolarian skeletons: Solution at depths. *Science*, *159*(3820), 1237–1239.

Bergmann, K. D., Finnegan, S., Creel, R., Eiler, J. M., Hughes, N. C., Popov, L. E., & Fischer, W. W. (2018). A paired apatite and calcite clumped isotope thermometry approach to estimating Cambro-Ordovician seawater temperatures and isotopic composition. *Geochimica Et Cosmochimica Acta*, *224*, 18–41. https://doi.org/10.1016/j.gca.2017.11.015

Berner, R. A. (1992). Weathering, plants, and the long-term carbon cycle. *Geochimica Et Cosmochimica Acta*, *56*(8), 3225–3231. https://doi.org/10.1016/0016-7037(92)90300-8

Berner, R. A., & Caldeira, K. (1997). The need for mass balance and feedback in the geochemical carbon cycle. *Geology*, *25*(10), 955–956. https://doi.org/10.1130/0091-7613(1997)025<0955:TNFMBA>2.3.CO;2

Boyce, C. K., & Lee, J. E. (2017). Plant evolution and climate over geological timescales. *Annual Review of Earth and Planetary Sciences*, *45*(1), 61–87. https://doi.org/10.1146/annurev-earth-063016-015629

Broecker, W. S., & Sanyal, A. (1998). Does atmospheric CO 2 police the rate of chemical weathering? *Global Biogeochemical Cycles*, *12*(3), 403–408.

Cardinal, D., Alleman, L. Y., Dehairs, F., Savoye, N., Trull, T. W., & André, L. (2005). Relevance of silicon isotopes to Si-nutrient utilization and Si-source assessment in Antarctic waters: Silicon isotopes in Antarctic waters. *Global Biogeochemical Cycles*, *19*(2), https://doi.org/10.1029/2004GB002364 GB2007.

Cassarino, L., Coath, C. D., Xavier, J. R., & Hendry, K. R. (2018). Silicon isotopes of deep sea sponges: New insights into biomineralisation and skeletal structure. *Biogeosciences*, *15*(22), 6959–6977. https://doi.org/10.5194/bg-15-6959-2018

Chen, K., Lü, X., Qian, Y., Wu, S., & Dong, S. (2020). δ30Si and δ18O of multiple silica phases in chert: Implications for δ30Siseawater of Darriwilian seawater and sea surface temperatures. *Palaeogeography, Palaeoclimatology, Palaeoecology*, *544*, 109584. https://doi.org/10.1016/j.palaeo.2020.109584

Chu, J. W. F., Maldonado, M., Yahel, G., & Leys, S. P. (2011). Glass sponge reefs as a silicon sink. *Marine Ecology Progress Series*, *441*, 1–14. https://doi.org/10.3354/meps09381

Cocks, L. R. M., & Torsvik, T. H. (2002). Earth geography from 500 to 400 million years ago: A faunal and palaeomagnetic review. *Journal of the Geological Society*, *159*(6), 631–644. https://doi.org/10.1144/0016-764901-118

Conley, D. J., Frings, P. J., Fontorbe, G., Clymans, W., Stadmark, J., Hendry, K. R., Marron, A. O., & De La Rocha, C. L. (2017). Biosilicification drives a decline of dissolved Si in the Oceans through geologic Time. *Frontiers in Marine Science*, *4*, 397. https://doi.org/10.3389/fmars.2017.00397

Crowley, T. J., & Baum, S. K. (1995). Reconciling late ordovician (440 Ma) glaciation with very high (14X) CO 2 levels. *Journal of Geophysical Research*, *100*(D1), 1093–1101.

Davies, N. S., & Gibling, M. R. (2010). Cambrian to devonian evolution of alluvial systems: The sedimentological impact of the earliest land plants. *Earth-Science Reviews*, *98*(3), 171–200. https://doi.org/10.1016/j.earscirev.2009.11.002

De La Rocha, C. L., & Bickle, M. J. (2005). Sensitivity of silicon isotopes to whole-ocean changes in the silica cycle. *Marine Geology*, *217*, 267–282. https://doi.org/10.1016/j.margeo.2004.11.016

de la Rocha, C. L., Brzezinski, M. A., & DeNiro, M. J. (1997). Fractionation of silicon isotopes by marine diatoms during biogenic silica formation. *Geochimica Et Cosmochimica Acta*, *61*(23), 5051–5056. https://doi.org/10.1016/S0016-7037(97)00300-1

Degens, E. T., & Epstein, S. (1962). Relationship between O^{18}/O^{16} ratios in coexisting carbonates, cherts, and diatomites. *AAPG Bulletin*, *46*(4), 534–542.

Ding, T. P., Gao, J. F., Tian, S. H., Fan, C. F., Zhao, Y., Wan, D. F., & Zhou, J. X. (2017). The δ^{30}Si peak value discovered in middle Proterozoic chert and its implication for environmental variations in the ancient ocean. *Scientific Reports*, *7*, 44000. https://doi.org/10.1038/srep44000

Egan, K. E., Rickaby, R. E. M., Hendry, K. R., & Halliday, A. N. (2013). Opening the gateways for diatoms primes earth for antarctic glaciation. *Earth and Planetary Science Letters*, *375*, 34–43. https://doi.org/10.1016/j.epsl.2013.04.030

Erez, J., Takahashi, K., & Honjo, S. (1982). In-situ dissolution experiment of radiolaria in the central North Pacific ocean. *Earth and Planetary Science Letters*, *59*(2), 245–254. https://doi.org/10.1016/0012-821X(82)90129-7

Ernst, W. G., & Calvert, S. E. (1969). An experimental study of the recrystallization of porcelanite and its bearing on the origin of some bedded cherts. *American Journal of Science*, *267-A*, 114–133.

Finnegan, S., Bergmann, K., Eiler, J. M., Jones, D. S., Fike, D. A., Eisenman, I., Hughes, N. C., Tripati, A. K., & Fischer, W. W. (2011). The magnitude and duration of late ordovician-early silurian glaciation. *Science*, *331*(6019), 903–906.

Fontorbe, G., Frings, P. J., De La Rocha, C. L., Hendry, K. R., Carstensen, J., & Conley, D. J. (2017). Enrichment of dissolved silica in the deep equatorial pacific during the eocene-oligocene: Equatorial pacific DSi enrichment. *Paleoceanography*, *32*(8), 848–863. https://doi.org/10.1002/2017PA003090

Fontorbe, G., Frings, P. J., De La Rocha, C. L., Hendry, K. R., & Conley, D. J. (2016). A silicon depleted North Atlantic since the Palaeogene: Evidence from sponge and radiolarian silicon isotopes. *Earth and Planetary Science Letters*, *453*, 67–77. https://doi.org/10.1016/j.epsl.2016.08.006

Fontorbe, G., Frings, P. J., De La Rocha, C. L., Hendry, K. R., & Conley, D. J. (2020). Constraints on earth system functioning at the paleocene-eocene thermal maximum from the marine silicon cycle. *Paleoceanography and Paleoclimatology*, *35*(5), 1616. https://doi.org/10.1029/2020PA003873

Fraser, T. A., Allen, T. L., Lane, L. S., & Reyes, J. C. (2012). Shale gas potential in north Yukon: Results from a diamond drillhole study in western Richardson Mountains. In K. E. MacFarlane, & P. J. Sack (Eds.). *Yukon exploration and geology 2011* (pp. 45–74). Yukon Geological Survey.

Frings, P. J., Clymans, W., Fontorbe, G., De La Rocha, C. L., & Conley, D. J. (2016). The continental Si cycle and its impact on the ocean Si isotope budget. *Chemical Geology*, *425*, 12–36. https://doi.org/10.1016/j.chemgeo.2016.01.020

Geilert, S., Vroon, P. Z., Roerdink, D. L., Van Cappellen, P., & van Bergen, M. J. (2014). Silicon isotope fractionation during abiotic silica precipitation at low temperatures: Inferences from flow-through experiments. *Geochimica Et Cosmochimica Acta*, *142*, 95–114. https://doi.org/10.1016/j.gca.2014.07.003

Georg, R. B., Halliday, A. N., Schauble, E. A., & Reynolds, B. C. (2007). Silicon in the Earth's core. *Nature*, *447*(7148), 1102–1106.

Gibling, M. R., & Davies, N. S. (2012). Palaeozoic landscapes shaped by plant evolution. *Nature Geoscience*, *5*(2), 99–105. https://doi.org/10.1038/ngeo1376

Gouretski, V. V., & Koltermann, K. P. (2006). The world ocean circulation experiment (WOCE) global hydrographic climatology. *UCAR/NCAR-Research Data Archive*, https://doi.org/10.5065/GS51-V170

Grenne, T., & Slack, J. F. (2003). Paleozoic and Mesozoic silica-rich seawater: Evidence from hematitic chert (jasper) deposits. *Geology*, *31*(4), 319–322. https://doi.org/10.1130/0091-7613(2003)031<0319:PAMSRS>2.0.CO;2

Harper, H. E., & Knoll, A. H. (1975). Silica, diatoms, and Cenozoic radiolarian evolution. *Geology*, *3*(4), 175–177. https://doi.org/10.1130/0091-7613(1975)3<175:SDACRE>2.0.CO;2

Harrison, K. G. (2000). Role of increased marine silica input on paleo-pCO2 levels. *Paleoceanography*, *15*(3), 292–298.

Heck, P. R., Huberty, J. M., Kita, N. T., Ushikubo, T., Kozdon, R., & Valley, J. W. (2011). SIMS analyses of silicon and oxygen isotope ratios for quartz from archean and paleoproterozoic banded iron formations. *Geochimica Et Cosmochimica Acta*, *75*(20), 5879–5891. https://doi.org/10.1016/j.gca.2011.07.023

Hendry, K. R., Cassarino, L., Bates, S. L., Culwick, T., Frost, M., Goodwin, C., & Howell, K. L. (2019). Silicon isotopic systematics of deep-sea sponge grounds in the North Atlantic. *Quaternary Science Reviews*, *210*, 1–14. https://doi.org/10.1016/j.quascirev.2019.02.017

Hendry, K. R., Georg, R. B., Rickaby, R. E. M., Robinson, L. F., & Halliday, A. N. (2010). Deep ocean nutrients during the last glacial maximum deduced from sponge silicon isotopic compositions. *Earth and Planetary Science Letters*, *292*(3), 290–300. https://doi.org/10.1016/j.epsl.2010.02.005

Hendry, K. R., & Robinson, L. F. (2012). The relationship between silicon isotope fractionation in sponges and silicic acid concentration: Modern and core-top studies of biogenic opal. *Geochimica Et Cosmochimica Acta*, *81*, 1–12. https://doi.org/10.1016/j.gca.2011.12.010

Hendry, K. R., Robinson, L. F., McManus, J. F., & Hays, J. D. (2014). Silicon isotopes indicate enhanced carbon export efficiency in the North Atlantic during deglaciation. *Nature Communications*, *5*, 3107. https://doi.org/10.1038/ncomms4107

Ibarra, D. E., Rugenstein, J. K. C., Bachan, A., Baresch, A., Lau, K. V., Thomas, D. L., Lee, J.-E., Boyce, C. K., & Chamberlain, C. P. (2019). Modeling the consequences of land plant evolution on silicate weathering. *American Journal of Science*, *319*(1), 1–43. https://doi.org/10.2475/01.2019.01

Jones, D. L., & Knauth, L. P. (1979). Oxygen isotopic and petrographic evidence relevant to the origin of the Arkansas Novaculite. *Journal of Sedimentary Research*, *49*(2), 581–597.

Kamatani, A. (1971). Physical and chemical characteristics of biogenous silica. *Marine Biology*, *8*(2), 89–95. https://doi.org/10.1007/BF00350922

Karhu, J., & Epstein, S. (1986). The implication of the oxygen isotope records in coexisting cherts and phosphates. *Geochimica Et Cosmochimica Acta*, *50*(8), 1745–1756. https://doi.org/10.1016/0016-7037(86)90136-5

Kastner, M., Keene, J. B., & Gieskes, J. M. (1977). Diagenesis of siliceous oozes—I. Chemical controls on the rate of opal-A to opal-CT transformation—an experimental study. *Geochimica Et Cosmochimica Acta*, *41*(8), 1041–1051.

Knauth, L. P., & Epstein, S. (1976). Hydrogen and oxygen isotope ratios in nodular and bedded cherts. *Geochimica Et Cosmochimica Acta*, *40*(9), 1095–1108. https://doi.org/10.1016/0016-7037(76)90051-X

Koning, E., Gehlen, M., Flank, A. M., Calas, G., & Epping, E. (2007). Rapid post-mortem incorporation of aluminum in diatom frustules: Evidence from chemical and structural analyses. *Marine Chemistry*, *106*(1), 208–222. https://doi.org/10.1016/j.marchem.2006.06.009

Lenz, A. C. (1972). Ordovician to devonian history of northern Yukon and adjacent district of Mackenzie. *Bulletin of Canadian Petroleum Geology*, *20*(2), 321–361.

Li, Y. H., Ding, T. P., & Wan, D. F. (1994). Experimental study of silicon isotope dynamic fractionation and its geological application. *Mineral Deposits*, *13*(3), 282–288.

Link, C. M., & Bustin, R. M. (1989). Organic maturation and thermal history of phanerozoic strata in northern Yukon and northwestern district of Mackenzie. *Bulletin of Canadian Petroleum Geology*, *37*(3), 266–292.

López-Acosta, M., Leynaert, A., Grall, J., & Maldonado, M. (2018). Silicon consumption kinetics by marine sponges: An assessment of their role at the ecosystem level: Silicate utilization by sponges. *Limnology and Oceanography*, *63*(6), 2508–2522. https://doi.org/10.1002/lno.10956

López-Acosta, M., Leynaert, A., & Maldonado, M. (2016). Silicon consumption in two shallow-water sponges with contrasting biological features: Si consumption by sponges. *Limnology and Oceanography*, *61*(6), 2139–2150. https://doi.org/10.1002/lno.10359

Loucaides, S., Michalopoulos, P., Presti, M., Koning, E., Behrends, T., & Van Cappellen, P. (2010). Seawater-mediated interactions between diatomaceous silica and terrigenous sediments: Results from long-term incubation experiments. *Chemical Geology*, *270*(1), 68–79. https://doi.org/10.1016/j.chemgeo.2009.11.006

Maldonado, M., Carmona, M. C., Velásquez, Z., Puig, A., Cruzado, A., López, A., & Young, C. M. (2005). Siliceous sponges as a silicon sink: An overlooked aspect of benthopelagic coupling in the marine silicon cycle. *Limnology and Oceanography*, *50*(3), 799–809. https://doi.org/10.4319/lo.2005.50.3.0799

Maldonado, M., Navarro, L., Grasa, A., Gonzalez, A., & Vaquerizo, I. (2011). Silicon uptake by sponges: A twist to understanding nutrient cycling on continental margins. *Scientific Reports*, *1*, 30. https://doi.org/10.1038/srep00030

Maliva, R. G., Knoll, A. H., & Siever, R. (1989). Secular change in chert distribution: A reflection of evolving biological participation in the silica cycle. *Palaios*, *4*, 519–532. https://doi.org/10.2307/3514743

Marin-Carbonne, J., Chaussidon, M., & Robert, F. (2012). Micrometer-scale chemical and isotopic criteria (O and Si) on the origin and history of precambrian cherts: Implications for paleo-temperature reconstructions. *Geochimica Et Cosmochimica Acta*, *92*, 129–147. https://doi.org/10.1016/j.gca.2012.05.040

Matheney, R. K., & Knauth, L. P. (1989). Oxygen-isotope fractionation between marine biogenic silica and seawater. *Geochimica Et*

Cosmochimica Acta, *53*(12), 3207–3214. https://doi.org/10.1016/0016-7037(89)90101-4

Matteuzo, M. C., Alexandre, A., Varajao, A. F. D. C., Volkmer-Ribiero, C., Almeida, A. C. S., Varajao, C. A. C., Vallet-Coulomb, C., Sonzogni, C., & Miche, H. (2013). Assessing the relationship between the δ18O signatures of siliceous sponge spicules and water in a tropical lacustrine environment (Minas Gerais, Brazil). *Biosciences Discussion*, *10*, 12887–12918.

McMahon, W. J., & Davies, N. S. (2018). Evolution of alluvial mudrock forced by early land plants. *Science*, *359*(6379), 1022–1024.

Michalopoulos, P., & Aller, R. C. (2004). Early diagenesis of biogenic silica in the Amazon delta: Alteration, authigenic clay formation, and storage. *Geochimica Et Cosmochimica Acta*, *68*(5), 1061–1085. https://doi.org/10.1016/j.gca.2003.07.018

Michalopoulos, P., Aller, R. C., & Reeder, R. J. (2000). Conversion of diatoms to clays during early diagenesis in tropical, continental shelf muds. *Geology*, *28*(12), 1095–1098. https://doi.org/10.1130/0091-7613(2000)28<1095:CODTCD>2.0.CO;2

Milligan, A. J., Varela, D. E., Brzezinski, M. A., & Morel, F. M. M. (2004). Dynamics of silicon metabolism and silicon isotopic discrimination in a marine diatomas a function of pCO2. *Limnology and Oceanography*, *49*(2), 322–329.

Morrow, D. W. (1999). *Lower Paleozoic stratigraphy of northern Yukon territory and northwestern district of Mackenzie*, Vol. *538*. Geological Survey of Canada.

Moulton, K. L., West, J., & Berner, R. A. (2000). Solute flux and mineral mass balance approaches to the quantification of plant effects on silicate weathering. *American Journal of Science*, *300*(7), 539–570. https://doi.org/10.2475/ajs.300.7.539

Murata, K. J., Friedman, I., & Gleason, J. D. (1977). Oxygen isotope relations between diagenetic silica minerals in monterey shale, temblor range, California. *American Journal of Science*, *277*(3), 259–272. https://doi.org/10.2475/ajs.277.3.259

Nelson, D. M., Goering, J. J., Kilham, S. S., & Guillard, R. R. L. (1976). Kinetics of silicic acid uptake and rates of silica dissolution in the marine diatom Thalassiosira pseudonana. *Journal of Phycology*, *12*(2), 246–252.

Pogge von Strandmann, P. A. E., Opfergelt, S., Lai, Y. J., Sigfússon, B., Gislason, S. R., & Burton, K. W. (2012). Lithium, magnesium and silicon isotope behaviour accompanying weathering in a basaltic soil and pore water profile in Iceland. *Earth and Planetary Science Letters*, *339–340*, 11–23. https://doi.org/10.1016/j.epsl.2012.05.035

Racki, G., & Cordey, F. (2000). Radiolarian palaeoecology and radiolarites: Is the present the key to the past? *Earth-Science Reviews*, *52*(1), 83–120. https://doi.org/10.1016/S0012-8252(00)00024-6

Reincke, T., & Barthel, D. (1997). Silica uptake kinetics of halichondria panicea in Kiel Bight. *Marine Biology*, *129*(4), 591–593. https://doi.org/10.1007/s002270050200

Roerdink, D. L., van den Boorn, S. H. J. M., Geilert, S., Vroon, P. Z., & van Bergen, M. J. (2015). Experimental constraints on kinetic and equilibrium silicon isotope fractionation during the formation of non-biogenic chert deposits. *Chemical Geology*, *402*, 40–51. https://doi.org/10.1016/j.chemgeo.2015.02.038

Schmidt, P., Bellot-Gurlet, L., Slodczyk, A., & Fröhlich, F. (2012). A hitherto unrecognised band in the Raman spectra of silica rocks: Influence of hydroxylated Si–O bonds (silanole) on the Raman moganite band in chalcedony and flint (SiO2). *Physics and Chemistry of Minerals*, *39*(6), 455–464. https://doi.org/10.1007/s00269-012-0499-7

Siever, R. (1991). Silica in the oceans; biological-geochemical interplay. In S. H. Schneider, & P. J. Boston (Eds.). *Scientists on Gaia* (pp. 287–295). MIT Press.

Siever, R. (1992). The silica cycle in the Precambrian. *Geochimica Et Cosmochimica Acta*, *56*(8), 3265–3272. https://doi.org/10.1016/0016-7037(92)90303-Z

Snelling, A. M., Swann, G. E. A., Pike, J., & Leng, M. J. (2014). Pliocene diatom and sponge spicule oxygen isotope ratios from the Bering Sea: Isotopic offsets and future directions. *Climate of the past Discussions*, *10*(3), 2087–2104.

Sperling, E. A., Robinson, J. M., Pisani, D., & Peterson, K. J. (2010). Where's the glass? Biomarkers, molecular clocks, and microRNAs suggest a 200-Myr missing Precambrian fossil record of siliceous sponge spicules. *Geobiology*, *8*(1), 24–36. https://doi.org/10.1111/j.1472-4669.2009.00225.x

Stefurak, E. J. T., Fischer, W. W., & Lowe, D. R. (2015). Texture-specific Si isotope variations in Barberton Greenstone Belt cherts record low temperature fractionations in early Archean seawater. *Geochimica Et Cosmochimica Acta*, *150*, 26–52. https://doi.org/10.1016/j.gca.2014.11.014

Strauss, J. V., Fraser, T., Melchin, M. J., Allen, T. J., Malinowski, J., Feng, X., Taylor, J. F., Day, J., Gill, B. C., & Sperling, E. A. (2020). The Road River group of northern Yukon, Canada: Early Paleozoic deep-water sedimentation within the great American carbonate bank. *Canadian Journal of Earth Sciences*, *57*(10), 1193–1219. https://doi.org/10.1139/cjes-2020-0017

Sutton, J. N., Varela, D. E., Brzezinski, M. A., & Beucher, C. P. (2013). Species-dependent silicon isotope fractionation by marine diatoms. *Geochimica Et Cosmochimica Acta*, *104*, 300–309. https://doi.org/10.1016/j.gca.2012.10.057

Tatzel, M., Stuff, M., Franz, G., Hippler, D., Wiechert, U., & von Blanckenburg, F. (2020). Siliceous sponge expansion and phosphogenesis in a shallow water environment in the Malyi Karatau range (Kazakhstan) during the Precambrian-Cambrian transition. *Precambrian Research*, *347*, 105830. https://doi.org/10.1016/j.precamres.2020.105830

Tatzel, M., von Blanckenburg, F., Oelze, M., Bouchez, J., & Hippler, D. (2017). Late Neoproterozoic seawater oxygenation by siliceous sponges. *Nature Communications*, *8*(1), 621. https://doi.org/10.1038/s41467-017-00586-5

Tatzel, M., von Blanckenburg, F., Oelze, M., Schuessler, J. A., & Bohrmann, G. (2015). The silicon isotope record of early silica diagenesis. *Earth and Planetary Science Letters*, *428*, 293–303. https://doi.org/10.1016/j.epsl.2015.07.018

Tréguer, P. (2002). Silica and the cycle of carbon in the ocean. *Comptes Rendus: Geoscience*, *334*(1), 3–11. https://doi.org/10.1016/S1631-0713(02)01680-2

Tréguer, P., & De La Rocha, C. L. (2013). The world ocean silica cycle. *Annual Review of Marine Science*, *5*, 477–501. https://doi.org/10.1146/annurev-marine-121211-172346

Tréguer, P., Nelson, D. M., Van Bennekom, A. J., Demaster, D. J., Leynaert, A., & Quéguiner, B. (1995). The silica balance in the world ocean: A reestimate. *Science*, *268*(5209), 375–379.

Trotter, J. A., Williams, I. S., Barnes, C. R., Lécuyer, C., & Nicoll, R. S. (2008). Did cooling oceans trigger Ordovician biodiversification? Evidence from conodont thermometry. *Science*, *321*(5888), 550–554.

Wille, M., Sutton, J., Ellwood, M. J., Sambridge, M., Maher, W., Eggins, S., & Kelly, M. (2010). Silicon isotopic fractionation in marine sponges: A new model for understanding silicon isotopic variations in sponges. *Earth and Planetary Science Letters*, *292*(3), 281–289. https://doi.org/10.1016/j.epsl.2010.01.036

Williams, L. A., & Crerar, D. A. (1985). Silica diagenesis; II, General mechanisms. *Journal of Sedimentary Research*, *55*(3), 312–321.

Williams, L. A., Parks, G. A., & Crerar, D. A. (1985). Silica diagenesis; I, Solubility controls. *Journal of Sedimentary Research*, *55*(3), 301–311.

Yanchilina, A. G., Yam, R., Kolodny, Y., & Shemesh, A. (2020). From opal-A ^{18}O to chert ^{18}O in deep sea sediments. *Geochimica Et Cosmochimica Acta*, *268*, 368–382.

Yanchilina, A. G., Yam, R., & Shemesh, A. (2021). The effect of sediment lithology on oxygen isotope composition and phase transformation

of marine biogenic opal. *Chemical Geology*, *570*, 120175. https://doi.org/10.1016/j.chemgeo.2021.120175

Zeebe, R. E., & Caldeira, K. (2008). Close mass balance of long-term carbon fluxes from ice-core CO2 and ocean chemistry records. *Nature Geoscience*, *1*(5), 312–315. https://doi.org/10.1038/ngeo185

Ziegler, K., Chadwick, O. A., Brzezinski, M. A., & Kelly, E. F. (2005). Natural variations of δ30Si ratios during progressive basalt weathering. *Hawaiian Islands*. *Geochimica Et Cosmochimica Acta*, *69*(19), 4597–4610. https://doi.org/10.1016/j.gca.2005.05.008

Ziegler, K., Chadwick, O. A., White, A. F., & Brzezinski, M. A. (2005). δ30Si systematics in a granitic saprolite. *Puerto Rico*. *Geology*, *33*(10), 817–820. https://doi.org/10.1130/G21707.1

SUPPORTING INFORMATION

Additional supporting information may be found online in the Supporting Information section.

How to cite this article: Trower EJ, Strauss JV, Sperling EA, Fischer WW. Isotopic analyses of Ordovician–Silurian siliceous skeletons indicate silica-depleted Paleozoic oceans. *Geobiology*. 2021;00:1–13. https://doi.org/10.1111/gbi.12449